LANGMUIR

pubs.acs.org/Langmuir Article

Polymer-Mediated Assembly from Core−Shell Particles to Tunable Structures and Microrotors

Jintao Tong,[#] Shihao Zang,[#] Jiayu Liu, Zhe Xu, Xianen Hu, Xiaojuan Bai, Xue Bai, Cheng Ma,* Wei Wang,* and Jianbin Huang*

Cite This: https://doi.org/10.1021/acs.langmuir.5c03874 Read Online

ACCESS | Metrics & More | Article Recommendations | Supporting Information

ABSTRACT: We introduce a polymer-mediated approach for assembling binary colloidal particles into core−shell and other tunable structures with their transformation into microrotors via Janus design. By mixing polyvinylpyrrolidone (PVP)-coated polystyrene (PS) microparticles with polymer-free silica nanoparticles, we exploit electrostatic repulsion to maintain dispersion until ionic screening permits a close approach. At this point, PVP acts as a molecular glue, selectively bridging bare silica onto PS surfaces to yield PS@SiO_2 core−shell structures. The number ratio of PS to SiO_2 dictates the assembly outcome. Excess PS leads to shared silica shells that link multiple cores into chains and colloidal gels, while excess silica leads to complete shell coverage and crystallization of microspheres into close-packed hexagonal lattices. Applying this method to Janus PS/Pt particles enables regioselective SiO_2 coating on the PS hemisphere only, producing asymmetric "PS@SiO_2"/Pt Janus microspheres that assemble into dimers and trimers through directional binding on the silica-coated hemispheres only. Remarkably, in 5% H_2O_2, the resulting Janus dimers transform into self-propelled microrotors that exhibit sustained rotation, powered by the catalytic decomposition of H_2O_2 on the exposed platinum hemispheres. These findings present a simple yet powerful strategy for the controlled synthesis of functional colloidal superstructures as well as stimulus-responsive micromachines.

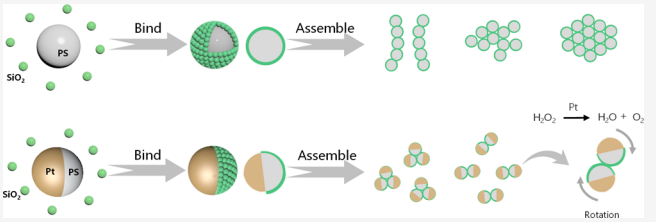

INTRODUCTION

Colloidal particles can serve as fundamental building blocks for self-assembly, enabling the construction of larger-scale structures and functional materials.[1−3] Among such systems, binary colloidal mixtures—comprising particles of distinct shapes, compositions, or sizes—have attracted broad interest for both fundamental research and applied technologies, including ionic crystals,[4−7] photonic crystals,[8−11] responsive gels,[12−14] and encapsulation systems.[15−17] When the size ratio between components is large, smaller particles often play a distinct role, leading to functional differentiation between the species. A classic example is a mixture of large colloidal particles with small silica nanoparticles (e.g., Ludox), where the smaller particles act as depletants, inducing effective attractions between the larger ones and promoting their condensation into ordered structures.[18−20]

However, when an attractive interaction force is introduced between the small and large components, the smaller particles begin to adhere to the surfaces of the larger ones. This process commonly leads to the formation of colloidosomes, structures in which a central colloidal core is fully coated with smaller satellite particles, resulting in a core−shell-like architecture.[21−23] Beyond these discrete assemblies, the smaller particles can also act as colloidal "glues", mediating directional interactions and promoting the organization of larger colloids into higher-order structures. While this concept holds potential for programmable self-assembly, practical examples that successfully harness such glue-like behavior remain rare. One prominent exception is DNA-mediated assembly,[24] which enables highly specific and tunable interactions; however, its complexity and high cost present substantial barriers to scalability for large-scale material fabrication.

Polymer-mediated interactions have recently emerged as a powerful strategy for inducing attraction between like-charged colloidal particles.[25−27] This mechanism typically involves a complementary pair: one particle coated with polymer chains and the other left polymer-free. Upon addition of salt to screen electrostatic repulsion, the particles can approach close enough for the polymer brushes to extend and adsorb onto the bare surface, forming an bridging interaction that effectively "glues" the particles together. A critical requirement for this strategy is the preservation of the polymer-free interface, which allows for selective adsorption and directional binding. To this end,

Received: July 27, 2025
Revised: September 25, 2025
Accepted: September 25, 2025
Published: October 9, 2025

certain amphiphilic block copolymers, such as Pluronic surfactants, are particularly effective, as they preferentially anchor to organic colloidal surfaces while leaving inorganic components accessible for bridging.[25]

Herein, we apply this polymer-mediated strategy to control the assembly of binary colloidal structures in which small particles act either as passive shell components or as active interparticle linkers, depending on the mixing ratio of both components. Specifically, we directly synthesized PVP-coated polystyrene (PS) microparticles and combined them with polymer-free silica nanoparticles (SiO_2) at a size ratio of approximately 20:1, initially stabilized by electrostatic repulsion. Upon ionic screening, the particles approach close enough for PVP chains to bridge and anchor silica onto PS surfaces. By varying the concentration of these two components (N_{PS} and N_{SiO_2}), we access four distinct structural regimes: (i) isolated PS@SiO_2 core−shell structures with complete shell coverage, (ii) chain-like and (iii) gel-like assemblies both through sharing of small particles, and (iv) crystalline arrays of core−shell particles.

Extended to Janus PS/Pt particles, this approach achieves regioselective SiO_2 deposition solely on the PS hemisphere, producing asymmetric "PS@SiO_2"/Pt colloids that can assemble into clusters (e.g., dimers or trimers), via directional attraction based on the silica-coated hemispheres (where SiO_2 acts as the "glue"). Intriguingly, these clusters immersed in 5% H_2O_2 exhibit sustained rotation driven by catalytic decomposition on the exposed platinum face. This work establishes a versatile approach where the polymer mediates the fabrication of core−shell particles and their reconfigurable assembly. Clusters assembled from Janus core−shell particles can be catalytically activated into microrotors, thereby advancing colloidal material development.

EXPERIMENTAL SECTION

Materials. Tetraethyl orthosilicate (TEOS), an ammonia solution (30 wt %), poly(acrylic acid), dichloromethane (DCM), and styrene were obtained from Aladdin Reagent. Fluorescein isothiocyanate (FITC), (3-aminopropyl) triethoxysilane (APTES), polyvinylpyrrolidone, sodium hydroxide, and potassium persulfate were purchased from Sigma-Aldrich Co.

Fabrication of Colloid Particles. *Synthesis of Silica Particles.* Monodisperse silica particles were synthesized using an optimized Stöber method.[28] First, silica seed particles (∼50 nm) were prepared by dissolving 2.5 mg of poly(acrylic acid) in 30 mL of ethanol, followed by the addition of 1.5 mL of an ammonia solution (30 wt %). Then, 0.75 mL of tetraethyl orthosilicate (TEOS) was slowly added using a syringe pump over 4 h under continuous stirring (700 rpm) at room temperature. After TEOS addition, stirring continued for 2 h. The resulting seed particles were used directly for subsequent experiments without further purification.

The further growth of SiO_2 particles was conducted in a 50 mL flask containing 24 mL of ethanol, 2 mL of water, 1.5 mL of an ammonia solution (30 wt %), and 6 mL of the seed SiO_2 sol prepared via the previous step. The mixture was placed on a magnetic stirrer at 700 rpm. Subsequently, 0.75 mL of tetraethyl orthosilicate (TEOS) was slowly added via a syringe pump over a period of 4 h. After the complete addition of TEOS, stirring continued for an additional 1 h. The resulting particles were collected by centrifugation. The particles collected by centrifugation were resuspended by ultrasonication in deionized water for 5 min, followed by centrifugation at 1000 rpm for 10 min. This cycle was repeated six times to thoroughly remove reaction byproducts and smaller secondary particles. Silica (diameter of 100 ± 10 nm) typically exhibited a ζ potential of approximately −40 mV, as measured with a Malvern Zetasizer Nano.

Synthesis of Fluorescently Labeled SiO_2 Particles. Fluorescent silica particles were prepared by covalent incorporation of FITC.[28] First, 1 mg of FITC was reacted with 5 mg of (3-aminopropyl) triethoxysilane (APTES) in 2 mL of ethanol under continuous stirring for 24 h at room temperature. Next, 6 mL of the SiO_2 suspension (100 ± 10 nm) from the previous step, 24 mL of ethanol, 2 mL of water, and 1.5 mL of ammonia were mixed in a 50 mL flask, and the mixture was stirred at 700 rpm. Ten cycles of dye incorporation were performed by sequential manual addition of 30 μL of TEOS and 5 μL of the FITC-APTES solution every 12 min. Following the reaction, the resulting fluorescently labeled SiO_2 particles were collected by centrifugation, washed three times with ethanol, and finally resuspended in deionized water for storage and further use.

Synthesis of PVP-Coated Polystyrene (PS) Particles. PVP-coated PS particles (∼2 μm) were synthesized by dispersion polymerization.[29] In a 250 mL three-neck flask equipped with a magnetic stir bar, 2.5 g of polyvinylpyrrolidone (PVP) was dissolved in 200 g of ethanol, followed by the addition of 25 mL of pretreated styrene, which was prewashed four times with 100 mL of a 10 wt % NaOH solution in a separatory funnel, then repeatedly washed with water until neutral, thoroughly dried over anhydrous magnesium sulfate, and stored at 4 °C. The mixture was stirred for 30 min and heated to 78 °C. Then, 180 mg of potassium persulfate (KPS, ≥99.0%, Sigma-Aldrich) dissolved in 5 mL of deionized water was added via syringe to initiate polymerization. After 12 h, seed particles (∼700 nm) were collected and washed by two cycles of sedimentation and resuspension in ethanol for seeded growth.

Then, 120 mL of a 1 wt % seed particle suspension was mixed with 40 mL of pretreated styrene in a 250 mL two-neck flask equipped with a magnetic stir bar. Subsequently, 50 mg of potassium persulfate dissolved in 2 mL of deionized water was added via a syringe. The suspension was heated to 78 °C and stirred for 24 h to produce PS particles with a diameter of ∼2 μm. The resulting particles were then washed three times by repeated centrifugation and redispersion in deionized water to remove small secondary nucleations. The PS−PVP core (∼2 μm) typically exhibited a ζ potential of approximately −30 mV, as measured with a Malvern Zetasizer Nano.

Synthesis of PVP-Free PS Particles. Micrometer-sized PS particles without a PVP polymer coating were synthesized via surfactant-free emulsion polymerization and seeded growth.[19,30] A mixture of 500 mL of deionized water, 60 mL of pretreated styrene as mentioned, and 0.5 g of KPS was stirred at 300 rpm in a three-neck flask at 78 °C overnight under nitrogen. The resulting seed particles were purified by three cycles of sedimentation and resuspension in deionized water.

For seeded growth, 120 mL of a 1 wt % seed suspension was mixed with 40 mL pretreated in a 250 mL two-neck flask. The mixture was purged with nitrogen and stirred for 1 h. Subsequently, 180 mg of KPS dissolved in 5 mL of water was injected via syringe. The suspension was heated to 78 °C and stirred at 300 rpm for 24 h. The resulting particles (∼2 μm) were washed three times by centrifugal washing with deionized water. PS cores typically exhibited a ζ potential of approximately −35 mV (Malvern Zetasizer Nano).

Fabrication of Janus PS/Pt Particles. Janus particles were fabricated by metal sputtering.[31] To fabricate Janus microspheres, the prepared PS (PVP) microspheres were dispersed in a mixture of ethanol and water in a volume ratio of 1:1. A 20 μL drop of the suspension was placed on a Si wafer tilted at 45° relative to the water surface. After a monolayer formed at the air−liquid interface, a 3 mM SDS surfactant solution was added to the water to stabilize the PS microsphere monolayer. During this process, SDS adsorption onto PS surfaces is unavoidable. However, when the fabricated particles are subsequently dispersed in abundant deionized water, the SDS concentration becomes negligible due to extreme dilution. Under these conditions, the measured ζ potential deviates by ≤5 mV from the inherent values of the PVP-coated PS, a difference falling within statistical error margins. Thus, the influence of SDS on particle surface properties can be considered to be negligible. The monolayer was then transferred to a preprepared Si wafer and dried in air.[32] Subsequently, a platinum (Pt) layer, approximately 20 nm in thickness, was sputter-coated onto the upper surface of the PS

https://doi.org/10.1021/acs.langmuir.5c03874
Langmuir XXXX, XXX, XXX−XXX

microsphere monolayer. This process was carried out using a high-vacuum sputtering system (Leica EM ACE600). The sputtering chamber was prefilled with argon gas and maintained at a vacuum level of 5×10^{-3} Torr.

Assembly of Colloid Particles. A 96-well cell plate (BeyoGold, 127 mm × 85 mm × 16 mm) containing the colloidal suspension was placed undisturbed on the microscope stage, allowing the micrometer-sized particles to sediment under gravity and equilibrate at a stable height above the substrate. At this point, a suspension of silica nanoparticles was added dropwise along with a stock NaCl solution (~50 mM), yielding a final concentration of ~5 mM in the dispersion. The dropwise addition protocol allows for the minimization of disturbance to the PS particles already dispersed near the substrate, and the system was equilibrated for 2 h to minimize diffusional effects from concentration gradients. By fine-tuning the number ratio of silica particles to PS core particles (as detailed in Figure 2a), a diverse range of microscopic configurations emerged continuously. Once the system reached equilibrium (after 2 h), data were collected. Number concentration N (inverse liters) of particles is calculated by original mass concentration M (grams per liter) measured with a microanalytical balance (Mettler Toledo, XPR2U) through gently drying, as follows: $N = 3M/(4\pi\rho r^3)$, where ρ is the particle density (assumed $\rho_{PS} = 1.05$ g/cm^3 and $\rho_{SiO_2} = 2.2$ g/cm^3) and r is the particle radius ($r_{PS} = 1 \times 10^{-4}$ cm, and $r_{SiO_2} = 5 \times 10^{-6}$ cm).

The interaction between binary particles (i.e., PS and SiO_2) is primarily governed by the competition between electrostatic repulsion and polymer-mediated bridging attraction. The interaction potential mediated by polymers was evaluated using numerical self-consistent field calculations.[33,34] This approach determines the interaction energy by computing the free energy difference between a state where particles are widely separated (no interaction) and a state at a specific distance of h. The expression is given by[35,36]

$$\frac{w(h)b^2}{k_BT} = \Omega(h) - \Omega(\infty) + N_p[u_p(h) - u_p(\infty)] \quad (1)$$

where b is the lattice size, defined as the distance between adjacent lattice points in the lattice model, N_p denotes the number of polymers anchored between the surfaces, $\Omega(h)$ and $u_p(h)$ represent the free energy and the chemical potential of the polymers, respectively, both dependent on interparticle distance h, and $\Omega(\infty)$ and $u_p(\infty)$ correspond to the grand potential of the system and the chemical potential of the polymers in an external bulk reservoir that is in equilibrium with the system, respectively.

Characterizations. Scanning electron microscopy (SEM) was performed by using a Carl Zeiss Supra 55 instrument with an energy-dispersive X-ray (EDX) analysis attachment. Samples for SEM analysis were drop-cast onto substrates, air-dried under ambient conditions, and sputter-coated with a 6 nm gold layer prior to imaging. Optical microscopy images and videos were acquired by using a Nikon 80i microscope. Fluorescence imaging was conducted with a Nikon A1R-si confocal laser scanning microscope (CLSM). Particle trajectories of spinning microrotors were analyzed by using PhysVis software and Python-based algorithms. ζ potential measurements were performed at 25 °C using a Zetasizer Nano ZS90 instrument.

RESULTS AND DISCUSSION

Polymer-Mediated Formation of Hybrid Core−Shell Structures. Conventional methods for fabricating colloidosome core−shell structures, like Pickering emulsification, rely on liquid droplets as soft templates to direct shell formation.[37] However, these approaches are often limited by sensitivity to particle wettability and emulsification conditions, leading to polydispersity in the resulting assemblies.[38] Microfluidic techniques offer improved uniformity,[39] but their scalability for large-scale production remains limited. Recently, polymer-mediated colloidal interactions have been explored as a versatile route to direct the assembly of hybrid structures through specific, tunable attractions between particles.[25,27]

In this study, the heteroaggregation process is based on two distinct components, organic PS cores (~2 μm) and inorganic silica shell particles (~100 nm), as illustrated in Figure 1a−c.

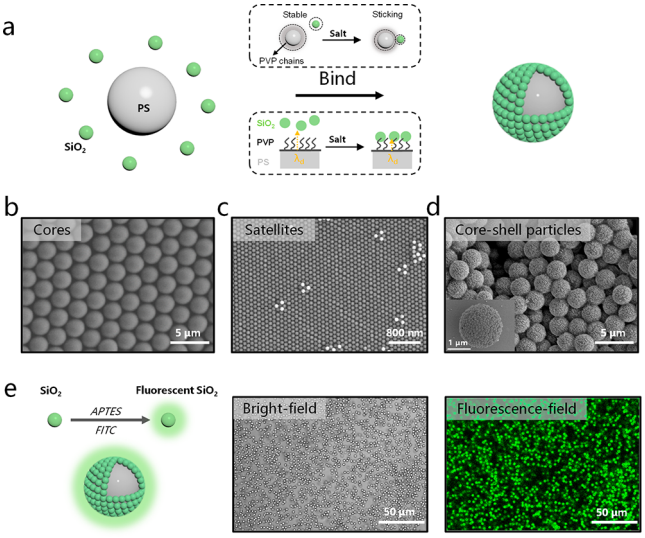

Figure 1. Polymer adsorption-based core−shell particles. (a) Schematic illustration of the polymer-mediated assembly process. Polyvinylpyrrolidone (PVP)-coated polystyrene (PS) cores (gray) selectively capture polymer-free silica nanoparticles (green) upon screening of electrostatic repulsion, as indicated by a reduction in Debye length (λ_d). Scanning electron microscopy (SEM) images of (b) PS cores and (c) silica satellites. (d) SEM image of assembled PS−silica core−shell particles. The inset shows a magnified view of a representative single colloidosome, showing uniform satellite coverage. (e) Confocal laser scanning microscopy (CLSM) image of colloidosomes with fluorescein isothiocyanate (FITC)-labeled silica, revealing a fluorescent shell surrounding the nonfluorescent PS core.

To engineer targeted attraction between the components, polyvinylpyrrolidone (PVP; $M \approx 50\,000$) was introduced as a dispersant during PS synthesis, resulting in surface-grafted PVP chains.[29,40] While molecular weight generally influences polymer brush length, this factor had little effect on the assembly process,[41] since the salt concentration of 5 mM is sufficient to screen the electrostatic repulsion and bring the particles into contact, as shown in Figure S1. As shown in Figure S2, energy-dispersive X-ray spectroscopy (EDX) confirms the presence of oxygen and nitrogen on the PS surface, consistent with PVP modification.

Upon the addition of concentrated silica nanoparticles into the PS suspension, the two species remain dispersed due to electrostatic repulsion. As shown in Figure 1a, introducing NaCl (concentration of ~5 mM) screens this repulsion, reducing the Debye length (λ_d) and allowing the particles to approach within a critical distance. At this range, PVP chains extending from the PS surface can adsorb onto the polymer-free silica particles, forming polymer bridges that drive specific attraction and promote assembly into colloidosomes, as shown in Figure 1d. While a decrease in electrostatic repulsion can mediate the assembly, reversibility is not achieved by its subsequent increase alone (e.g., via dialysis), as evidenced in Figure S3. This may be due to the molecular adhesion force between the polymer and surface,[42] and then the electrostatic

https://doi.org/10.1021/acs.langmuir.5c03874
Langmuir XXXX, XXX, XXX−XXX

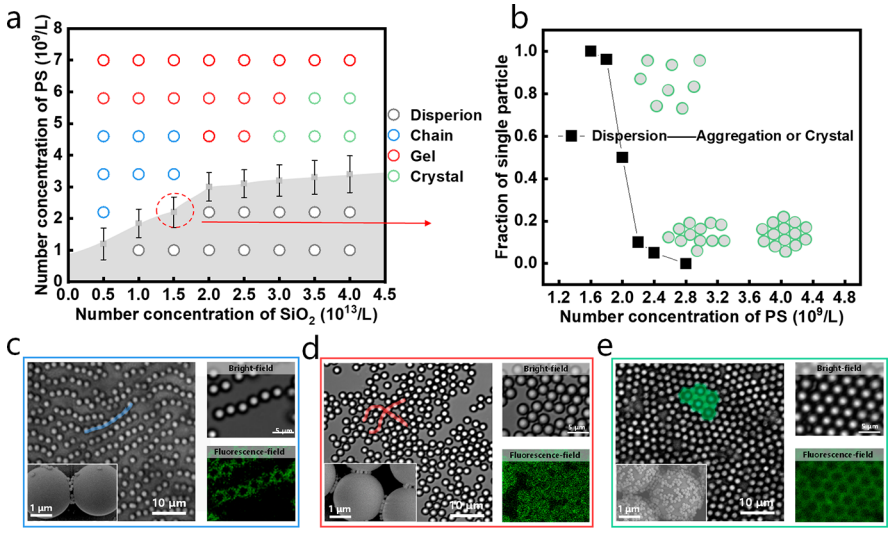

Figure 2. Tunable assembly outcomes. (a) Phase diagram illustrating the assembly behavior of binary colloidal mixtures as a function of the PS:SiO_2 number ratio. (b) Example of the boundary equilibrium measurement of the fraction of a single particle (f_{single} at a silica concentration of 1.5×10^{13} L^{-1}). (c) Chain-like assemblies formed via shared silica satellites. In the inset, a SEM image showing a single layer of shared-shell particles. (d) Gel-like structures formed via shared silica satellites. In the inset, a SEM image shows a single layer of shared-shell particles. (e) Crystalline arrays under CLSM observation. In the inset, a SEM image shows double layers of silica particles between adjacent PS cores. Notably, to minimize three-dimensional aggregation caused by solvent evaporation, the particle concentration used for SEM imaging was reduced compared to that used for fluorescence imaging while maintaining the same ratio between the two species.

repulsion is not strong enough to separate the particles. This approach can be extended to shell particles of other sizes (Figure S4).

To suppress intercore aggregation via shared silica bridges, an excess of silica is required. The degree of silica adsorption per PS core scales with the overall silica concentration (Figure S5). As illustrated in Figure 1e, fluorescent labeling of silica particles with FITC reveals a distinct fluorescent corona around the nonfluorescent PS cores, confirming in situ shell formation. Conversely, PS particles lacking PVP fail to form colloidosomes and instead exhibit nonspecific aggregation, as illustrated in Figure S6. Notably, selective cross-linking of the silica satellites, followed by etching of the PS core, yields a hollow shell structure (Figure S7), showing the potential for encapsulation and artificial transmembrane carriers.[16,23,43]

Similarly, polymer-mediated attraction can also be induced by introducing amphiphilic block copolymers—such as Pluronic F127, F108, and Brij-S100—into suspensions of unmodified PS (Figure S8). These surfactants spontaneously adsorb due to their architecture. The hydrophobic poly(propylene oxide) (PPO) segments anchor to PS, while hydrophilic poly(ethylene oxide) (PEO) segments extend into the aqueous phase, forming a steric layer.[5,25] Thereby, this polymer-mediated approach offers a modular and scalable route for assembling hybrid colloidosomes with tunable surface coverage and compatibility across a wide range of colloidal systems.

Tunable Assembly of Binary Colloidal Particles. The assembly of binary colloidal particles exhibits a pronounced dependence on the PS:SiO_2 number ratio, enabling tunable structure as depicted in Figure 2a. The phase boundaries are determined by counting the fraction of single particles (f_{single}) after the system equilibrates for 2 h, after which we quantified f_{single} from the fields of view of typically 1000 core particles total, as illustrated in Figure 2b. We classify gray as "dispersed core−shell" when $f_{single} \geq 0.9$ and green/blue as "chain/gel/crystal" when $f_{single} \leq 0.1$. The phase boundary is at $0.1 < f_{single} < 0.9$, which is denoted as the error bar. When the PS:SiO_2 number ratio > 1:5800, the limited availability of silica satellites promotes a distinct assembly regime in which adjacent PS cores become interconnected by shared satellites, leading to the formation of extended chains and colloidal gel networks, as shown in panels c and d of Figure 2 and Figure S9. Zoomed-in SEM imaging reveals a single layer of silica particles bridging neighboring PS cores, suggesting that bridging occurs at the interstitial sites. The formation mechanism of such chain structures may be a kinetically controlled process under thermal fluctuations. When the number concentration of larger PS particles falls below the gel network's threshold ($\sim 4.6 \times 10^9$ L^{-1}), PS particles are sparsely connected, resulting in relatively short chains. Based on our current understanding and within the scope of our expertise, we propose that the process may be primarily governed by a random assembly mechanism controlled by the number ratio. However, the detailed dynamics of this process remain an open question for further investigation.

In contrast, when the N_{PS}/N_{SiO_2} falls below 1/5800, indicating excess silica, two distinct assembly outcomes emerge, governed by the absolute PS concentration. At low PS number concentrations ($N_{PS} < 3.4 \times 10^9$ L^{-1} (gray region in Figure 2a)), discrete PS@SiO_2 colloidosomes form, consistent with observations mentioned in Figure 1. At higher PS concentrations ($N_{PS} \geq 3.4 \times 10^9$ L^{-1} (green region in Figure 2a)), the system transitions into crystalline arrays of partially coated core−shell particles, as shown in Figure 2e and Figure S10. Zoomed-in SEM imaging reveals double layers of silica particles between adjacent PS cores. Limitations in crystal size and uniformity originate primarily from polydispersity and heterogeneity in shell formation. Further improvements will focus on enhancing the structural order by optimizing particle uniformity and assembly conditions.

The mechanism of ordered assembly lies in the adsorption of small particles onto the surfaces of large particles, forming a

https://doi.org/10.1021/acs.langmuir.5c03874
Langmuir XXXX, XXX, XXX−XXX

core−shell structure that significantly increases the composite particle density. This enhances gravitational sedimentation, thereby facilitating easier two-dimensional ordered arrangement of particles near the substrate, whereas the depletion effects induced by small particles are insufficient to assemble, as shown in Figure S11. Meanwhile, moderate electrostatic repulsion (5 mM NaCl; $\lambda_d \approx 4.3$ nm) plays a key balancing role in maintaining the ordered structure and preventing disordered aggregation, as shown in Figure S12.

The observed phase transition boundary originates from distinct assembly outcomes determined by the PS:SiO_2 number ratio. At a fixed SiO_2 concentration, when the number of PS particles significantly exceeds the number of available SiO_2 binding sites, intense competition for shared SiO_2 shells leads to rapid random cross-linking, trapping the system in a nonequilibrium gel-like network. As the PS concentration decreases, the more balanced PS:SiO_2 ratio results in partially covered PS particles linked directionally by SiO_2, which may form chain-like assemblies. Only at a sufficiently low PS concentration (e.g., $N_{PS}/N_{SiO_2} < 1/5800$) does SiO_2 become clearly in excess, allowing each PS particle to be fully enveloped by SiO_2 nanoparticles and to form discrete, thermodynamically stable core−shell particles. Complementary structural characterization through CLSM (Figure 2c−e) and radial distribution function $g(r)$ (Figure S13) provide direct visualization evidence that confirms the structural programmability achieved through the mixing ratio of the components. This establishes number concentration-mediated assembly as a robust strategy for fabricating both disordered and crystalline colloidal architectures from identical building blocks. In contrast to conventional approaches—such as DNA-mediated assembly, which requires costly sequence design and functionalization, or depletion-driven assembly, which typically demands substantial background depletants and offers limitations on fixing the structure—our polymer-based approach offers a cost-effective alternative. By simply modulating the electrostatic interactions and predesign of a pair of polymer-grafted and polymer-free colloids, our strategy allows scalable and on-demand modulation of interactions without external fields. Furthermore, tuning the concentration ratio of the two species enables control over the assembly structures.

Assembly of the Janus Core−Shell Particles and Active Microrotors. Janus PS/Pt particles featuring a 20 nm thick Pt hemispherical layer could be deposited via magnetron sputtering (Figure 3a), as evidenced by the SEM image in Figure 3b. When this polymer-mediated strategy is applied to Janus PS/Pt particles, regioselective silica adsorption is achieved. Silica nanoparticles adsorb exclusively onto the PVP-coated PS hemisphere while avoiding the Pt-coated side (Figure 3c,d), yielding asymmetric colloidosome architectures (Janus "PS@SiO_2"/Pt).

At a higher Janus:silica number ratio (exceeding 1/3000), where silica acts as active interparticle linkers, dimers and trimers predominantly form with varied geometries, as detailed in Figure 4a−c. Fluorescence imaging confirms the fluorescent silica coverage and shared-shell connections in these assemblies, as shown in Figure 4b. At the optimized number ratio ($N_{PS/Pt}/N_{SiO_2} \approx 1/2000$), uniform dimers are obtained (Figure 4d). The inset of the CLSM merged view highlights a representative dimer where two Janus particles are joined by a continuous fluorescent shell, indicating a bridging mechanism mediated by shared silica satellites.

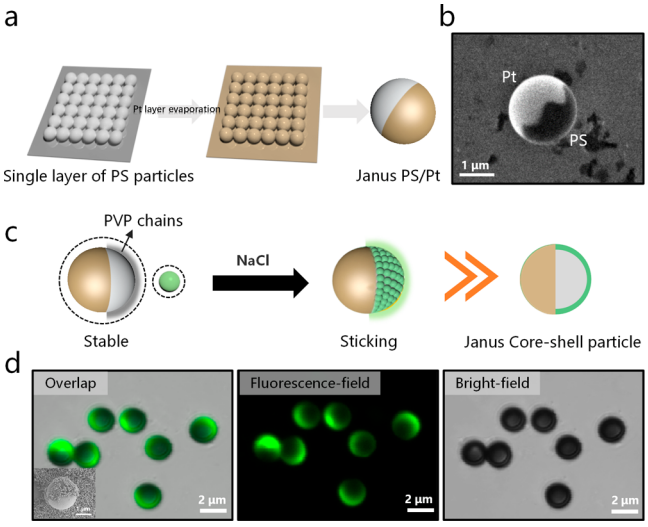

Figure 3. Janus core−shell particles. (a) Schematic illustration of Janus PS/Pt particle fabrication via platinum deposition onto polystyrene spheres. (b) SEM image of Janus PS/Pt particles with a hemispherical Pt coating; the darker side is PS. (c) Schematic of polymer-mediated, regioselective silica adsorption onto the PS hemisphere of Janus particles. (d) CLSM image showing Janus "PS@SiO_2"/Pt particles, with selective fluorescence on the PS side. In the inset, the corresponding SEM image confirms the asymmetric silica coating.

Beyond structural assembly, these Janus PS/Pt particles serve as self-propelled micromotors in a hydrogen peroxide (H_2O_2) solution, driven by Pt-catalyzed self-electrophoresis[44,45] (Video S1), whereas symmetric PS@SiO_2 particles without Pt catalytic sites exhibit only Brownian motion (Video S2). Previous studies have shown that controlled assembly of Janus particles enables rotational motion via symmetry breaking and directed torque generation.[46−48] Inspired by this concept, we observe that Janus "PS@SiO_2"/Pt dimers spontaneously transform into autonomous microrotors when suspended in 5 wt % H_2O_2 (Figure 4d−f and Video S3).

A simplified physical model can be constructed to understand the rotational behavior of the dimer: two identical spheres in contact along the x-axis, where each Janus particle is represented by drawing cross planes through its center, with the contact parts corresponding to the silica-coated polystyrene (PS) sides (Figure S14). The Pt-catalyzed self-electrophoretic propulsion generates a force directed from the platinum hemisphere toward the PS hemisphere, aligning with the normal vector of the Janus interface (denoted as $F1$, $F2$). Assuming equal magnitudes of propulsion, each force vector can be decomposed into components along the x-axis and within the orthogonal y−z plane. Rotational behavior arises when the projections of these vectors in the y−z plane satisfy $F1_{yz} \cdot F2_{yz} < 0$. In the ideal case of pure rotation without translation, the forces are equal and opposite $F1 = -F2$, canceling in the axial direction and driving the tangential rotation. Thus, dimer rotation originates from the antiparallel projection of propulsion forces within the plane perpendicular to the contact axis, with pure rotation achieved when the two Janus particles are symmetrically arranged around the point of contact.

https://doi.org/10.1021/acs.langmuir.5c03874
Langmuir XXXX, XXX, XXX−XXX

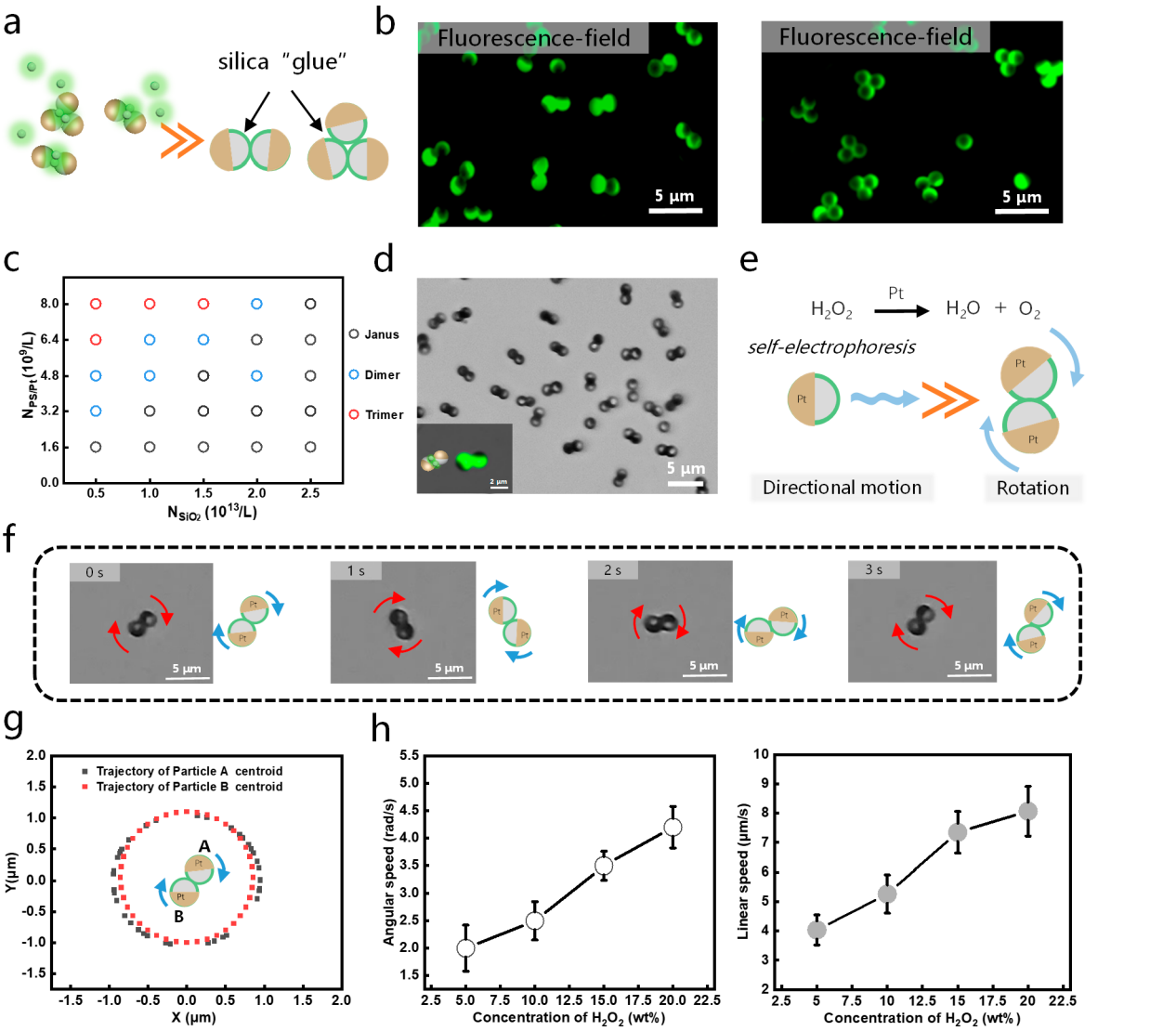

Figure 4. Assembly of the Janus core−shell particles and a microrotor. (a) Schematic illustration of Janus "PS@SiO_2"/Pt particle assembly into clusters. (b) Fluorescence images of dimers and trimers. (c) Phase diagram illustrating the assembly behavior of binary colloidal mixtures (Janus PS/Pt and SiO_2 particles) as a function of the Janus:silica number ratio (black circles denote Janus core−shell particles, blue circles dimers, and red circles trimers). (d) Optical microscopy image of dimers (the inset shows a CLSM merged view of a single dimer). (e) Schematic mechanism of a microrotor from a dimer through Pt-catalyzed reactions. (f) Representative snapshots from a microrotor motion video. (g) Centroid trajectory tracking for two particles within a dimer. (h) Dimer angular velocity (left, white circle) and linear velocity (right, gray circle) as a function of H_2O_2 concentration.

Since the relative orientation of the two Janus particles is set stochastically at assembly, the sign of the net torque—and thus rotation direction (i.e., clockwise vs counterclockwise)—is random. Only around 20% of the dimers exhibit persistent rotational motion (Figure S15) but can be further concentrated by waiting for the other dimers moving directionally away. However, this method cannot achieve complete separation of the inactive dimers. Tracking the center-of-mass trajectories of the two Janus particles reveals nearly circular, concentric trajectories with the rotation center located at the silica junction, confirming the in situ rotational behavior of the dimeric microrotor (Figure 4g). As depicted in Figure 4h, at a H_2O_2 concentration of 5 wt %, the dimers exhibit an average angular velocity of ∼2 rad/s and a linear velocity of ∼4 μm/s. Notably, the Janus dimer remains stable over the 4 h observation period, with no dissociation observed, while the loss of rotation is fuel-limited, as illustrated in Figure S16. Moreover, with an increase in H_2O_2 concentration, both the angular velocity (white circle, left axis) and the linear velocity (gray circle, right axis) increase.

In contrast, trimers exhibit a markedly reduced motility. Due to the triangular configuration and the force balance among the three propulsion vectors, the net torque is effectively canceled in most cases. The geometrical stability of the trimer suppresses rotational degrees of freedom, and only a small fraction (no more than 6% (Figure S12)) of trimers display sustained rotation under the same conditions.

These self-assembled microrotors act as active components in microrobotic systems, with potential uses in localized fluid mixing,[49,50] particle transport,[51] and drug delivery.[52,53] Although the hydrogen peroxide environment used here is not biocompatible, our assembly strategy is universal and can inform the design using alternative, biocompatible propulsion schemes (e.g., enzymatic,[54] magnetic,[55] or acoustic[56]).

https://doi.org/10.1021/acs.langmuir.5c03874
Langmuir XXXX, XXX, XXX−XXX

CONCLUSIONS

This work establishes a polymer-mediated paradigm for binary colloidal particles to construct core−shell and other tunable architectures. Charge screening reduces electrostatic repulsion, enabling PVP-coated PS cores to selectively capture SiO_2 particles for scalable fabrication of core−shell structures. By varying the concentration of these two components, we access four distinct structural regimes: (i) isolated PS@SiO_2 core−shell structures with complete shell coverage, (ii) chain-like and (iii) gel-like assemblies both through sharing of small particles, and (iv) crystalline arrays of core−shell particles. The extension of Janus PS/Pt systems utilizes surface asymmetry for regioselective SiO_2 adsorption, further generating clusters (dimers/trimers) via shared SiO_2. Importantly, the Pt-catalyzed decomposition of H_2O_2 creates antiparallel driving forces that transform static dimers into rotating microrotors with persistence. This method provides a simple and scalable approach for binary particles to create core−shell colloids and other tunable assemblies (e.g., crystals of core−shell particles and dimer-based microrotors). These resulting structures demonstrate potential for applications in fields such as photonic crystals and microfluidic transport.

ASSOCIATED CONTENT

Supporting Information

The Supporting Information is available free of charge at https://pubs.acs.org/doi/10.1021/acs.langmuir.5c03874.

Figures S1−S16 (PDF)

Video S1 (MP4)

Video S2 (MP4)

Video S3 (MP4)

AUTHOR INFORMATION

Corresponding Authors

Cheng Ma − *Beijing National Laboratory for Molecular Sciences (BNLMS) State Key Laboratory for Structural Chemistry of Unstable and Stable Species, College of Chemistry and Molecular Engineering, Peking University, Beijing 100871, P. R. China*; Email: 2406592570@pku.edu.cn

Wei Wang − *School of Materials Science and Engineering, Harbin Institute of Technology (Shenzhen), Shenzhen, Guangdong 518055, P. R. China*; Email: weiwangsz@hit.edu.cn

Jianbin Huang − *Beijing National Laboratory for Molecular Sciences (BNLMS) State Key Laboratory for Structural Chemistry of Unstable and Stable Species, College of Chemistry and Molecular Engineering, Peking University, Beijing 100871, P. R. China*; Email: jbhuang@pku.edu.cn

Authors

Jintao Tong − *Beijing National Laboratory for Molecular Sciences (BNLMS) State Key Laboratory for Structural Chemistry of Unstable and Stable Species, College of Chemistry and Molecular Engineering, Peking University, Beijing 100871, P. R. China*; orcid.org/0009-0009-5754-327X

Shihao Zang − *Department of Chemistry, New York University, New York, New York 10003, United States*; orcid.org/0000-0003-3996-8265

Jiayu Liu − *School of Materials Science and Engineering, Harbin Institute of Technology (Shenzhen), Shenzhen, Guangdong 518055, P. R. China*

Zhe Xu − *Department of Chemistry, New York University, New York, New York 10003, United States*; orcid.org/0000-0002-8599-079X

Xianen Hu − *Beijing National Laboratory for Molecular Sciences (BNLMS) State Key Laboratory for Structural Chemistry of Unstable and Stable Species, College of Chemistry and Molecular Engineering, Peking University, Beijing 100871, P. R. China*

Xiaojuan Bai − *Beijing National Laboratory for Molecular Sciences (BNLMS) State Key Laboratory for Structural Chemistry of Unstable and Stable Species, College of Chemistry and Molecular Engineering, Peking University, Beijing 100871, P. R. China*

Xue Bai − *Beijing National Laboratory for Molecular Sciences (BNLMS) State Key Laboratory for Structural Chemistry of Unstable and Stable Species, College of Chemistry and Molecular Engineering, Peking University, Beijing 100871, P. R. China*

Complete contact information is available at: https://pubs.acs.org/10.1021/acs.langmuir.5c03874

Author Contributions

#J.T. and S.Z. contributed equally to this work and also denoted as co-first authors. J.H. supervised and directed research. W.W. supervised the research on Janus particles and microrotors and provided insightful suggestions for revising the manuscript. J.T. designed and performed experiments with the assistance of S.Z., J.L., and X.H. J.T. and S.Z. wrote the paper. J.T., C.M., S.Z., Z.X., Xiaojuan Bai, and Xue Bai discussed the results and analyzed the data.

Notes

The authors declare no competing financial interest.

ACKNOWLEDGMENTS

This work is supported by the National Natural Science Foundation of China (22272002 and T2322006).

REFERENCES

(1) Poon, W. Colloids as big atoms. *Science* **2004**, *304*, 830−831.

(2) Boles, M. A.; Engel, M.; Talapin, D. V. Self-assembly of colloidal nanocrystals: from intricate structures to functional materials. *Chem. Rev.* **2016**, *116*, 11220−11289.

(3) Li, Z.; Fan, Q.; Yin, Y. Colloidal self-assembly approaches to smart nanostructured materials. *Chem. Rev.* **2022**, *122*, 4976−5067.

(4) Zang, S.; Hauser, A. W.; Paul, S.; Hocky, G. M.; Sacanna, S. Enabling three-dimensional real-space analysis of ionic colloidal crystallization. *Nat. Mater.* **2024**, *23*, 1131−1137.

(5) Hueckel, T.; Hocky, G. M.; Palacci, J.; Sacanna, S. Ionic solids from common colloids. *Nature* **2020**, *580*, 487−490.

(6) Leunissen, M.; Christova, C.; Hynninen, A. P.; Royall, C. P.; Campbell, A. I.; Imhof, A.; Dijkstra, M.; van Roij, R.; van Blaaderen, A. Ionic colloidal crystals of oppositely charged particles. *Nature* **2005**, *437*, 235−240.

(7) Zang, S.; Paul, S.; Leung, C. W.; Chen, M. S.; Hueckel, T.; Hocky, G. M.; Sacanna, S. Direct observation and control of non-classical crystallization pathways in binary colloidal systems. *Nat. Commun.* **2025**, *16*, 3645.

(8) Cai, Z.; Li, Z.; Ravaine, S.; He, M.; Song, Y.; Yin, Y.; Zheng, H.; Teng, J.; Zhang, A. From colloidal particles to photonic crystals: advances in self-assembly and their emerging applications. *Chem. Soc. Rev.* **2021**, *50*, 5898−5951.

(9) Iakobson, O.; Ivan'kova, E.; Shevchenko, N. Photonic crystal films based on polymer particles with a core/shell structure responding to ethanol. *Langmuir* **2023**, *39*, 9952−9962.
(10) Liu, J.; Nero, M.; Jansson, K.; Willhammar, T.; Sipponen, M. H. Photonic crystals with rainbow colors by centrifugation-assisted assembly of colloidal lignin nanoparticles. *Nat. Commun.* **2023**, *14*, 3099.
(11) Hensley, A.; Jacobs, W. M.; Rogers, W. B. Self-assembly of photonic crystals by controlling the nucleation and growth of DNA-coated colloids. *Proc. Natl. Acad. Sci. U. S. A.* **2022**, *119*, No. e2114050118.
(12) Chen, H.; Nofen, E. M.; Rykaczewski, K.; Dai, L. L. Colloidal lattices of environmentally responsive microgel particles at ionic liquid-water interfaces. *J. Colloid Interface Sci.* **2017**, *504*, 440−447.
(13) Jiang, Y.; Seto, R. Colloidal gelation with non-sticky particles. *Nat. Commun.* **2023**, *14*, 2773.
(14) Minami, S.; Suzuki, D.; Urayama, K. Rheological aspects of colloidal gels in thermoresponsive microgel suspensions: formation, structure, and linear and nonlinear viscoelasticity. *Curr. Opin. Colloid Interface Sci.* **2019**, *43*, 113−124.
(15) Bollhorst, T.; Rezwan, K.; Maas, M. Colloidal capsules: nano- and microcapsules with colloidal particle shells. *Chem. Soc. Rev.* **2017**, *46*, 2091−2126.
(16) Dinsmore, A. D.; Hsu, M. F.; Nikolaides, M. G.; Marquez, M.; Bausch, A. R.; Weitz, D. A. Colloidosomes: selectively permeable capsules composed of colloidal particles. *Science* **2002**, *298*, 1006−1009.
(17) Evers, C.; Luiken, J.; Bolhuis, P.; Kegel, W. K. Self-assembly of microcapsules via colloidal bond hybridization and anisotropy. *Nature* **2016**, *534*, 364−368.
(18) Onuh, G.; Harries, D.; Manor, O. Depletion-induced self-assembly of colloidal particles on a solid substrate. *Langmuir* **2024**, *40*, 8554−8561.
(19) Liu, M. Z.; Zheng, X. L.; Grebe, V.; Pine, D. J.; Weck, M. Tunable assembly of hybrid colloids induced by regioselective depletion. *Nat. Mater.* **2020**, *19*, 1354−1361.
(20) Youssef, M.; Hueckel, T.; Yi, G. R.; Sacanna, S. Shape-shifting colloids via stimulated dewetting. *Nat. Commun.* **2016**, *7*, 12216.
(21) Xie, X.; Zhang, W.; Abbaspourrad, A.; Ahn, J.; Bader, A.; Bose, S.; Weitz, D. A.; Anderson, D. G.; et al. Microfluidic fabrication of colloidal nanomaterials-encapsulated microcapsules for biomolecular sensing. *Nano Lett.* **2017**, *17*, 2015−2020.
(22) Phadtare, S.; Kumar, A.; Vinod, V. P.; Dash, C.; Palaskar, D. V.; Rao, M.; Shukla, P. G.; Sivaram, S.; Sastry, M. Direct assembly of gold nanoparticle "shells" on polyurethane microsphere "cores" and their application as enzyme immobilization templates. *Chem. Mater.* **2003**, *15*, 1944−1949.
(23) Xu, Z.; Hueckel, T.; Irvine, W. T.; Sacanna, S. Caged Colloids. *Chem. Mater.* **2023**, *35*, 6357−6363.
(24) Girard, M.; Wang, S.; Du, J. S.; Das, A.; Huang, Z.; Dravid, V. P.; Lee, B.; Mirkin, C. A.; Olvera de la Cruz, M. Particle analogs of electrons in colloidal crystals. *Science* **2019**, *364*, 1174−1178.
(25) Opdam, J.; Tuinier, R.; Hueckel, T.; Snoeren, T. J.; Sacanna, S. Selective colloidal bonds via polymer-mediated interactions. *Soft Matter* **2020**, *16*, 7438−7446.
(26) Evans, R.; Napper, D. H. Flocculation of latices by low molecular weight polymers. *Nature* **1973**, *246*, 34−35.
(27) Gong, Z.; Hueckel, T.; Yi, G. R.; Sacanna, S. Patchy particles made by colloidal fusion. *Nature* **2017**, *550*, 234−238.
(28) Khlebtsov, B. N.; Burov, A. M. Synthesis of monodisperse silica particles by controlled regrowth. *Colloid J.* **2023**, *85*, 456−468.
(29) Ha, S.; Park, O.; Im, S. H. Size control of highly monodisperse polystyrene particles by modified dispersion polymerization. *Macromol. Res.* **2010**, *18*, 935−943.
(30) Telford, A.; Pham, B.; Neto, C.; Hawkett, B. S. Micron-sized polystyrene particles by surfactant-free emulsion polymerization in air: Synthesis and mechanism. *J. Polym. Sci., Part A: Polym. Chem.* **2013**, *51*, 3997−4002.
(31) Liu, J.; Yang, Z.; Yan, Z.; Duan, S.; Chen, X.; Cui, D.; Cao, D.; Kuang, T.; Ma, X.; Wang, W. Chemical micromotors move faster at oil-water interfaces. *J. Am. Chem. Soc.* **2024**, *146*, 4221−4233.
(32) Chen, Y. K.; Li, H.; Chen, J. M.; Li, D.; Zhang, M. Y.; Yu, G. H.; Jiang, L.; Zong, Y.; Dong, B.; Zeng, Z. F.; Wang, Y. D.; Chi, L. F. Self-generating nanogaps for highly effective surface-enhanced Raman spectroscopy. *Nano Res.* **2022**, *15*, 3496−3503.
(33) Scheutjens, J. M.; Fleer, G. J. Statistical theory of the adsorption of interacting chain molecules. 1. Partition function, segment density distribution, and adsorption isotherms. *J. Phys. Chem.* **1979**, *83*, 1619−1635.
(34) Scheutjens, J. M.; Fleer, G. J. Statistical theory of the adsorption of interacting chain molecules. 2. Train, loop and tail size distribution. *J. Phys. Chem.* **1980**, *84*, 178−190.
(35) Fleer, G. J.; Scheutjens, J. M. Block copolymer adsorption and stabilization of colloids. *Colloids Surf.* **1990**, *51*, 281−298.
(36) Opdam, J.; Tuinier, R.; Hueckel, T.; Snoeren, T. J.; Sacanna, S. Selective colloidal bonds via polymer-mediated interactions. *Soft Matter* **2020**, *16*, 7438−7446.
(37) Xu, X. W.; Zhang, X. M.; Liu, C.; Yang, Y. L.; Liu, J. W.; Cong, H. P.; Dong, C. H.; Ren, X. F.; Yu, S. H. One-pot colloidal chemistry route to homogeneous and doped colloidosomes. *J. Am. Chem. Soc.* **2013**, *135*, 12928−12931.
(38) Jiang, H.; Sheng, Y.; Ngai, T. Pickering emulsions: Versatility of colloidal particles and recent applications. *Curr. Opin. Colloid Interface Sci.* **2020**, *49*, 1−15.
(39) Kim, S. H.; Weitz, D. A. One-Step Emulsification of multiple concentric shells with capillary microfluidic devices. *Angew. Chem., Int. Ed.* **2011**, *123*, 8890−8893.
(40) Menshikova, A. Y.; Evseeva, T. G.; Skurkis, Y.; Tennikova, T. B.; Ivanchev, S. Monodisperse carboxylated polystyrene particles: synthesis, electrokinetic and adsorptive properties. *Polymer* **2005**, *46*, 1417−1425.
(41) Youssef, M.; Morin, A.; Aubret, A.; Sacanna, S.; Palacci, J. Rapid characterization of neutral polymer brush with a conventional zetameter and a variable pinch of salt. *Soft Matter* **2020**, *16*, 4274−4282.
(42) Vander Beek, G. P.; Stuart, M. A. C.; Fleer, G. J.; Hofman, J. E. Segmental adsorption energies for polymers on silica and alumina. *Macromolecules* **1991**, *24*, 6600−6611.
(43) Xu, Z.; Hueckel, T.; Irvine, W. T.; Sacanna, S. Transmembrane transport in inorganic colloidal cell-mimics. *Nature* **2021**, *597*, 220−224.
(44) Wang, Y.; Hernandez, R. M.; Bartlett, D. J.; Bingham, J. M.; Kline, T. R.; Sen, A.; Mallouk, T. E. Bipolar electrochemical mechanism for the propulsion of catalytic nanomotors in hydrogen peroxide solutions. *Langmuir* **2006**, *22*, 10451−10456.
(45) Howse, J. R.; Jones, R. A.; Ryan, A. J.; Gough, T.; Vafabakhsh, R.; Golestanian, R. Self-motile colloidal particles: From random walks to directed propulsion and chemotaxis. *Phys. Rev. Lett.* **2007**, *99*, 048102.
(46) Ebbens, S.; Jones, R. A. L.; Ryan, A. J.; Golestanian, R.; Howse, J. R. Self-assembled autonomous runners and tumblers. *Phys. Rev. E* **2010**, *82*, 015304.
(47) Gao, W.; Pei, A.; Feng, X.; Hennessy, C.; Wang, J. Organized self-assembly of Janus micromotors with hydrophobic hemispheres. *J. Am. Chem. Soc.* **2013**, *135*, 998−1001.
(48) Lyu, X. L.; Chen, J. Y.; Zhu, R. T.; Liu, J. Y.; Fu, L. S.; Moran, J. L.; Wang, W. Active synthetic microrotors: Design strategies and applications. *ACS Nano* **2023**, *17*, 11969−11993.
(49) Koehler, J.; Ghadiri, R.; Ksouri, S. I.; Guo, Q.; Gurevich, E. L.; Ostendorf, A. Generation of microfluidic flow using an optically assembled and magnetically driven microrotor. *J. Phys. D: Appl. Phys.* **2014**, *47*, 505501.
(50) Kokot, G.; Das, S.; Winkler, R. G.; Gompper, G.; Aranson, I. S.; Snezhko, A. Active turbulence in a gas of self-assembled spinners. *Proc. Natl. Acad. Sci. U.S.A.* **2017**, *114*, 12870−12875.
(51) Kim, K.; Liang, Z.; Liu, M.; Fan, D. E. Biobased High-performance rotary micromotors for individually reconfigurable

https://doi.org/10.1021/acs.langmuir.5c03874
Langmuir XXXX, XXX, XXX−XXX

micromachine arrays and microfluidic applications. *ACS Appl. Mater. Interfaces* **2017**, *9*, 6144−6152.
(52) Wu, Z.; Troll, J.; Jeong, H.-H.; Wei, Q.; Stang, M.; Ziemssen, F.; Wang, Z.; Dong, M.; Schnichels, S.; Qiu, T.; Fischer, P. A swarm of slippery micropropellers penetrates the vitreous body of the eye. *Sci. Adv.* **2018**, *4*, No. eaat4388.
(53) Wang, D.; Gao, C.; Wang, W.; Sun, M.; Guo, B.; Xie, H.; He, Q. Shape-transformable, fusible rodlike swimming liquid metal nanomachine. *ACS Nano* **2018**, *12*, 10212−10220.
(54) Arqué, X.; Romero-Rivera, A.; Feixas, F.; Patiño, T.; Osuna, S.; Sánchez, S. Intrinsic enzymatic properties modulate the self-propulsion of micromotors. *Nat. Commun.* **2019**, *10*, 2826.
(55) Zhou, H.; Mayorga-Martinez, C. C.; Pané, S.; Zhang, L.; Pumera, M. Magnetically driven micro and nanorobots. *Chem. Rev.* **2021**, *121*, 4999−5041.
(56) Rao, K. J.; Li, F.; Meng, L.; Zheng, H.; Cai, F.; Wang, W. A force to be reckoned with: a review of synthetic microswimmers powered by ultrasound. *Small* **2015**, *11*, 2836−21846.

https://doi.org/10.1021/acs.langmuir.5c03874
Langmuir XXXX, XXX, XXX−XXX